A model and experimental approach to the middle ear transfer function related to hearing in the humpback whale (Megaptera novaeangliae)

Andrew A. Tubelli, Aleksandrs Zosuls, Darlene R. Ketten, and David C. Mountain

Citation: The Journal of the Acoustical Society of America **144**, 525 (2018); doi: 10.1121/1.5048421
View online: https://doi.org/10.1121/1.5048421
View Table of Contents: http://asa.scitation.org/toc/jas/144/2
Published by the Acoustical Society of America

A model and experimental approach to the middle ear transfer function related to hearing in the humpback whale (*Megaptera novaeangliae*)

Andrew A. Tubelli,[a] Aleksandrs Zosuls,[b] Darlene R. Ketten, and David C. Mountain[c]
Boston University Hearing Research Center and Department of Biomedical Engineering, 44 Cummington Mall, Boston, Massachusetts 02215, USA

(Received 31 March 2018; revised 29 June 2018; accepted 11 July 2018; published online 1 August 2018)

At present, there are no direct measures of hearing for any baleen whale (Mysticeti). The most viable alternative to *in vivo* approaches to simulate the audiogram is through modeling outer, middle, and inner ear functions based on the anatomy and material properties of each component. This paper describes a finite element model of the middle ear for the humpback whale (*Megaptera novaeangliae*) to calculate the middle ear transfer function (METF) to determine acoustic energy transmission to the cochlea. The model was developed based on high resolution computed tomography imaging and direct anatomical measurements of the middle ear components for this mysticete species. Mechanical properties for the middle ear tissues were determined from experimental measurements and published values. The METF for the humpback whale predicted a better frequency range between approximately 15 Hz and 3 kHz or between 200 Hz and 9 kHz based on two potential stimulation locations. Experimental measures of the ossicular chain, tympanic membrane, and tympanic bone velocities showed frequency response characteristics consistent with the model. The predicted best sensitivity hearing ranges match well with known vocalizations of this species.

https://doi.org/10.1121/1.5048421

[WWA] Pages: 525–535

I. INTRODUCTION

Little is known about the impact of anthropogenic noise on baleen whales (Cetacea, suborder Mysticeti). Unlike toothed whales (Cetacea, suborder Odontoceti), for which there are behavioral and electrophysiological methods for direct measures of the audiograms of multiple species, there are currently no practical methods for reliable *in vivo* measures of the auditory thresholds of mysticetes.

The humpback whale (*Megaptera novaeangliae*) is a species of concern because their critical habitats coincide with ocean areas heavily used by humans for recreation, transport, industrial, exploratory, and military purposes. Multiple studies on the vocalizations of humpback whales have been published (e.g., Payne *et al.*, 1983; Silber, 1986; Thompson *et al.*, 1986; Clark, 1990; Au *et al.*, 2006). While it is expected that this species hears well at or near the peak frequencies of these emitted sounds, vocalizations by many vertebrate species are known to have significant features at frequencies outside of the peak spectra of their vocalizations (Dooling *et al.*, 1979; Ladich and Yan, 1998; Meenderink *et al.*, 2010). Peak spectra are often near but not coincident with best hearing sensitivities. Further, vocalizations typically do not cover the entire range of hearing. For example, the bottlenose dolphin (*Tursiops truncatus*) has a total hearing range based on audiometric data of approximately 100 Hz to 160 kHz, while their whistles are typically between 1 kHz to 24 kHz and clicks between 30 kHz and 60 kHz (see Wartzok and Ketten, 1999). It is also usual for hearing ranges to include vocalization frequencies related to predation and many abiotic signals in addition to the frequencies of conspecific vocalizations (Ketten, 2002). Therefore, vocalizations give us some indication but they alone do not provide sufficient information for determining hearing ranges or sensitivities. For this reason, we must understand the receptor capabilities.

Given the lack of available auditory threshold measurements and current inability to make direct audiometric measurements, functional auditory system models derived from anatomical and physical properties of ear tissues offer the best insight into mysticete hearing. The audiogram can be thought of as the synergistic response of the functional elements of each major division of the ear (external, middle, and inner ear) to incoming acoustic signals (Dallos, 1973; Rosowski, 1991; Ruggero and Temchin, 2002). By building a series of models estimating the output at each functional division of the ear, we obtain a composite estimated audiogram for species for which there is no experimentally measured live data counterpart. The external and middle ears largely contribute to determining range of best sensitivity and the bandwidth of the audiogram (Olson, 1998; Overstreet and Ruggero, 2002; Ravicz *et al.*, 2008), while

[a]Current address: Broad Institute of MIT and Harvard, 415 Main Street, Cambridge, MA 02142, USA. Electronic mail: atubelli@bu.edu
[b]Also at: Biology Department, Woods Hole Oceanographic Institution, 266 Woods Hole Road, Woods Hole, MA 02543, USA.
[c]Posthumous

the basilar membrane and cochlear structure dictate total possible hearing range and the high-frequency cutoff (Ruggero and Temchin, 2002) as well as low-frequency cutoffs (Manoussaki *et al.*, 2008).

Extensive descriptions of whale ear anatomy are available (e.g., Lillie, 1910; Yamada, 1953; Fraser and Purves, 1960; Ketten, 2000; Mead and Fordyce, 2009; Ekdale *et al.*, 2011). We provide here a brief summary of key features. The functional elements of the inner ear and middle ear (cochlear labyrinth and ossicular chain) have essentially the same format as found in terrestrial mammals. The ear complex of cetaceans differs in that the fundamental ear structures are housed in two dense, connected bones: the tympanic and periotic bones that are wholly or partially decoupled from the skull. The tympanic bone is a hollow, shell-shaped bone that forms the middle ear cavity and contains the three ossicles with associated ligaments, nerves, and spongy mucosal tissues (corpus cavernosum). The periotic bone contains the cochlear and vestibular labyrinths. The tympanic and periotic bones are fused at their posterior edges, forming the tympano-periotic complex, which is positioned extracranially. The complex is attached to a groove in the skull by a bony flange of the periotic. The tympanic membrane (referred to commonly as a "glove finger" based on its elongated, hollow, everted shape) projects laterally into the ear canal and has a conical wax cap at its tip (Fraser and Purves, 1960; Ketten, 2000). The ear canal extends laterally and posteriorly, paralleling the bony flange and is narrow and largely occluded with wax and debris.

It is yet undetermined exactly how sound is conducted to the ear in most cetaceans including mysticetes. The extensive anatomical level of development of the middle ear structures and particularly the tympanic membrane argues against the middle ear being dysfunctional and that transmission to the cochlea is principally by bone conduction, as argued by Cranford and Krysl (2015). We also know that middle ear ligaments and tissues, particularly the stapedial muscle, are well developed in baleen whales as well as in all odontocete species that have been examined (Fleischer, 1978; McCormick *et al.*, 1980; Pilleri *et al.*, 1987; Ketten, 1992; Ketten, 1994). Further, as in odontocetes, specialized elongated bundles of fats exist in mysticetes that are aligned with the jaw and terminate on the tympano-periotic complex on or near the tympanic membrane (Yamato *et al.*, 2012).

In a previous study, we modeled the middle ear of the minke whale (*Balaenoptera acutorostrata*) (Tubelli *et al.*, 2012) computationally using the finite element (FE) method, where geometries of varying complexity are broken up into elements and solved for numerically. This method has been used to study the middle ears of multiple species of terrestrial mammals (Koike *et al.*, 2002; Gan *et al.*, 2004; Homma *et al.*, 2009; Homma *et al.*, 2010; Wang and Gan, 2016; De Greef *et al.*, 2017). The current study builds on this prior demonstration of the application of established FE work for the minke whale by Tubelli *et al.* (2012), employing the same methods but with higher resolution models to increase our accuracy for assessing the hearing range in the humpback whale via the middle ear transfer function (METF). Experimentally-measured data taken directly on middle ears from this same species are also presented to further assist with interpreting the model results.

II. FE MODEL

A. Anatomical reconstruction

A comprehensive middle ear reconstruction was created as a composite of separate reconstructions from computed tomography scan data sets from three different humpback whale ear specimens of similar size (e.g., measured lengths at the sigmoid processes and mallei were within 7% of each other) and condition. By combining the scan data, we optimized the quality of individual tissues represented in the composite reconstruction. Specimens employed in the project were obtained in collaboration with the Mid-Atlantic and New England regions of the US stranding network. The ears were collected by stranding network responders during necropsies of beached carcasses in North Carolina, New York, and Massachusetts. After collection, the ear tissues were sent to Woods Hole Oceanographic Institution (WHOI) for analysis under letters of authorization and US Fish and Wildlife service/National Marine Fisheries Services permits (932-1489-08, 493-1848-00, 493-1848-02, 130062, and 130062-1) issued to D. R. Ketten, WHOI. The carcasses were designated Code 3 (moderate decomposition) by the responders at time of necropsy. The specimens employed for this study consisted of ears from a yearling female, subadult female, and an adult male. Additional information on the specimens is provided in Table I.

All ears were scanned using a Volume Zoom Spiral Scanner (Siemens AG, Munich) with ultra-high bone and mid soft tissue kernels. Scans were obtained using a 0.5 mm spiral acquisition at 120 KV and 240 mA with the ears aligned for transaxial images paralleling the cochlear midmodiolar plane. Baseline images were formatted at 0.1 mm isotropic voxels throughout the entire tympano-periotic complex. Secondary images were obtained as well from anisotropic reformatted images with $0.2 \times 0.2 \times 0.5$ mm voxels. Multiplanar reformats were also produced in orthogonal views with reconstructions and reformatted reslicing to provide ultra-high-resolution images of the ossicular chain regions. Both raw acquisition data and all DICOM images were archived for each ear.

TABLE I. Specimens used in this study.

Specimen	Side	Sex	Age	Condition of tissue	Function in this study
Mnov22	Left	M	Adult	Code 3 (moderate decomposition)	Model (TM) and experimental
Mnov26	Left	F	Yearling	Code 3 (moderate decomposition)	Model (bone and interossicular joints)
Mnov31	Right	F	Subadult	Code 3 (moderate decomposition)	Model (suspensory soft tissue)

Regions and structures of interest in the DICOM image stack were segmented using the software program AMIRA (Mercury Computer Systems, Chelmsford, MA). The segmented regions for *M. novaeangliae* middle ears include bone (malleus, incus, stapes, and tympanic bone), articular soft tissue (incudomalleolar joint and incudostapedial joint), tympanic membrane, suspensory soft tissue (the posterior incudal ligament that connects the incus to the periotic bone and the stapedius tendon that connects the stapedius muscle to the head of the stapes), and annular ligament of the oval window (Fig. 1). Segmented regions from each of the three reconstructed ears were selected according to the health or integrity of the post mortem tissues. One specimen was used for only the tympano-periotic bone reconstruction as some soft tissues had sufficient post mortem artifacts that they were deemed unreliable for accurate measures. Of the two other scan data sets, one provided a well preserved, reliable representation for the tympanic membrane reconstruction, and the other additional data on the stapedial tendon and posterior incudal ligament measures and insertion points. Anatomical measurements of lengths and angles of the tissues were obtained during post-scan dissections to confirm the accuracy of the reconstructions. One suspensory tissue that was observed in the minke whale by Tubelli *et al.* (2012), the tensor tympani tendon, was not observed in any of the *M. novaeangliae* specimens that were dissected; however, we cannot definitively conclude from these samples that the tensor tympani muscle is absent in the humpback whale.

B. FE analysis

The geometry of both reconstructions was retopologized in Maya (Autodesk Inc., San Rafael, CA) to better fit the contour of the models. The finalized geometry of the *M. novaeangliae* reconstruction contained 26615 triangular surface elements.

Linear FE analysis of the middle ear model was performed using COMSOL Multiphysics (COMSOL Inc., Stockholm). The surface geometry translated to a mesh consisting of 49423 tetrahedral elements using COMSOL's free mesher and solved within the software to determine the frequency response between 1 Hz and 100 kHz.

C. Material properties

Almost none of the material properties of interest have been directly measured for *M. novaeangliae*, but using existing literature and knowledge of anatomical similarities, we can estimate physiologically relevant values for these properties. Table II summarizes the values used for the humpback whale middle ear model. All materials were modeled as linear and isotropic.

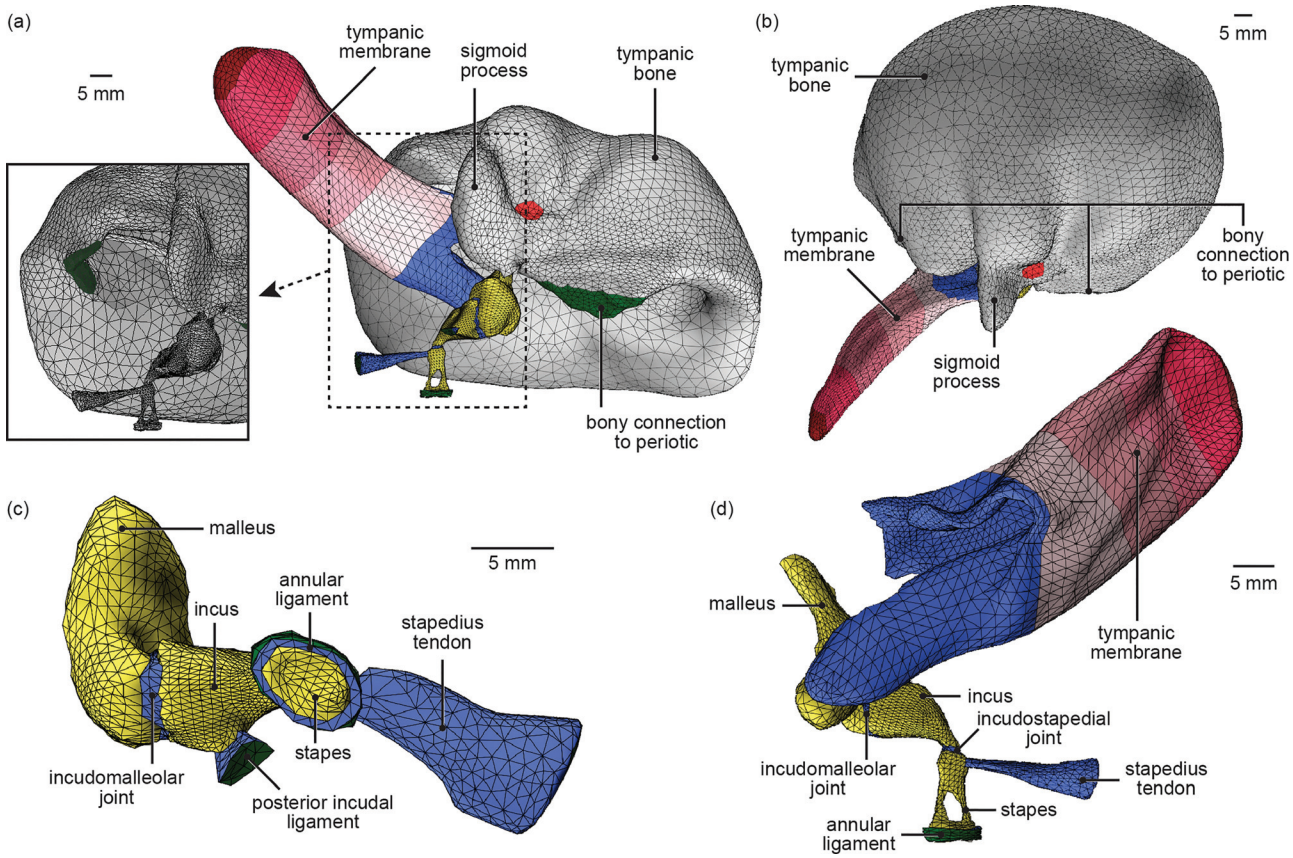

FIG. 1. Labeled mesh of the humpback whale middle ear model. (a) Lateral view, inset has the same view with tympanic membrane removed to show one of the bony connections to the periotic bone, (b) ventral view, (c) dorsal view (tympanic membrane and tympanic bone hidden), and (d) medial view (tympanic bone hidden). Also shown are fixed boundary conditions (distal edges of soft tissues and bony connections to periotic bone, in green), and input areas (variations of red) for the tympanic bone and gradation of input locations for the tympanic membrane used for sensitivity analysis. The middle shade of red to the tip of the tympanic membrane indicates the area used in the base model.

TABLE II. Material property values for the *M. novaeangliae* model. See text for sources.

Component	Young's modulus (N/m^2)	Density (kg/m^3)	Poisson's ratio
Tympanic bone	3.50×10^{10}	2.30×10^3	0.3
Malleus	3.50×10^{10}	2.30×10^3	0.3
Incus	3.50×10^{10}	2.30×10^3	0.3
Stapes	3.50×10^{10}	2.30×10^3	0.3
Tympanic membrane/tympanic ligament	1.35×10^7	1.32×10^3	0.45
Annular ligament	2.90×10^5	1.32×10^3	0.45
Stapedial tendon	1.00×10^7	1.32×10^3	0.45
Posterior incudal ligament	1.00×10^7	1.32×10^3	0.45
Incudostapedial joint	1.00×10^7	1.32×10^3	0.45
Incudomalleolar joint	1.00×10^7	1.32×10^3	0.45

1. Young's modulus of bone

Young's modulus, the ratio of stress to strain that describes the stiffness of a material, of bone in the model was based on nanoindentation measurements from Tubelli *et al.* (2014). That study did not include measurements for humpback whale ossicles; however, in considering a single value of Young's modulus for all bone that assumed uniformity, two groups of values emerged: a higher Young's modulus for odontocetes averaging around 60 GPa and a lower Young's modulus for mysticetes averaging around 35 GPa. If we assume that these values are representative of those for other species in the suborders, then the average of mysticete measurements can be employed as the Young's modulus value for humpback whale middle ear bones.

2. Bone density

Bone densities for *M. novaeangliae* middle ear ossicles measured by Nummela *et al.* (1999) ranged from 2.27×10^3 to $2.33 \times 10^3\,kg/m^3$ depending on the structure measured. An average value of $2.30 \times 10^3\,kg/m^3$ was used here across all bony regions in the model.

To further assess whether this value is appropriate to use for humpback whale middle ear bone, an estimate of density was calculated by measuring the mass of each ossicle from one humpback whale specimen and the corresponding volume computationally measured from the reconstruction of those same ossicles. Density was estimated to be within 11.6%, 8.3%, and 1.3% of the average value noted above for the malleus, incus, and stapes, respectively; therefore, we can reasonably conclude that the average M. *novaeangliae* middle ear bone density calculated from Nummela *et al.* (1999) is a sufficient model value.

3. Young's modulus of soft tissue

Since there are no direct measurements of Young's moduli for soft tissues of the ear in any species, we must take one of two approaches: rely on parameter values used in other middle ear models that were based on tuning model output data to experimental results or estimate them based on the range of values for any directly measured mammalian soft tissues. In previous FE studies, Young's modulus values used for ligaments and tendons were on the order of a megapascal plus or minus one order of magnitude (e.g., Koike *et al.*, 2002; Gan *et al.*, 2004; Homma *et al.*, 2010; De Greef *et al.*, 2017). Experimentally measured values of soft tissue Young's moduli, the majority of which are for ligaments and tendons in the knee and shoulder of humans, are generally on the order of hundreds of megapascals (e.g., Stäubli *et al.*, 1999; McGough *et al.*, 1996; Provenzano *et al.*, 2002; Hashemi *et al.*, 2005; Chandrashekar *et al.*, 2006). The reason for the discrepancy between experimentally measured Young's moduli and model-derived values is unclear. Sensitivity analysis of soft tissue Young's moduli was performed within this range (0.1–900 MPa) of values to determine how these changes affect the middle ear frequency response.

For the humpback whale middle ear model, a base value of 10 MPa was used across all soft tissues, with the exception of the annular ligament and the tympanic membrane. The annular ligament was consistently lower in most middle ear models and is treated separately here because of its unique fiber orientation (Fleischer, 1978). The value used for the base model was 0.29 MPa, an average of four other middle ear model studies (De Greef *et al.*, 2017; Homma *et al.*, 2010; Koike *et al.*, 2002; Wang and Gan, 2016). The model value used for annular ligament is 3% of the suspensory and articular soft tissue value. This ratio was kept for sensitivity analysis when testing low and high values: 3 kPa and 27 MPa, respectively. The value of Young's modulus for the tympanic membrane was the same used for the minke whale Tubelli *et al.* (2012) based on the observation that the structure is most similar to the pars flaccida of the terrestrial mammalian tympanic membrane (Fraser and Purves, 1954). Sensitivity analysis of Young's modulus for the tympanic membrane was performed within the same range as soft tissue parametric analysis (0.1–900 MPa) to address effects of parameter value uncertainty on the model.

4. Soft tissue density

To estimate soft tissue density, we similarly investigated previous FE studies as well as directly measured density values from the literature. Most of the middle ear FE model density values were traced back to sources that used an assumption rather than direct measurements. Rather than relying on assumption, we used an average value calculated from direct measurements of tendinous tissue density from various non-auditory terrestrial mammalian tendons in the literature ($1.32 \times 10^3\,kg/m^3$) (Ker, 1981; Kuo *et al.*, 2001; Hashemi *et al.*, 2005).

5. Poisson's ratio

In the model, a value of 0.3 was used for Poisson's ratio (a ratio of transverse strain to longitudinal strain) for bone; this value is commonly used for bone in middle ear models (e.g., Gan *et al.*, 2004; Homma *et al.*, 2010). Since soft tissue is nearly incompressible, a Poisson's ratio value of 0.45 was used as it is closer to that of an incompressible material, similar to Qi *et al.* (2006) and Tuck-Lee *et al.* (2008).

D. Boundary conditions

Because of uncertainty of how sound reaches the middle ear, an input pressure was tested on two separate areas resulting in two separate models. These two models are here referred to as the tympanic bone (TB) model and the tympanic membrane (TM) model. For the TB model, an input pressure was applied to a region 37.32 mm^2 adjacent to the sigmoid process, a projecting ridge on the lateral surface of the tympanic bone. This region of bone is a region near where specialized fats that are thought to act as a preferential sound path to the ear contact the tympano-periotic complex and tympanic membrane in the minke whale (Yamato *et al.*, 2012) and odontocetes (Norris, 1968; Ketten, 2000). The second region of input tested in the TM model was the tympanic membrane itself (see Fig. 1). Given the hypertrophied "glove finger" structure of the tympanic membrane in mysticetes and its firm attachment to the manubrium of the malleus, it is arguable that this elaborate tympanic membrane has some involvement in mysticete hearing. The surface areas of stimulation of the tympanic membrane, based on surrounding anatomy and potentially based on frequency, could range anywhere from the membrane tip which abuts a ceruminous or wax cap (Purves, 1955) to the entire length of the non-ligamentous portion external to the middle ear cavity. The area used for the base METF was in the middle of these extremes, 1710 mm^2. Four additional input areas, from the small tip area to the full membrane area within the auditory canal, were examined via sensitivity analysis. These input areas are shown in Fig. 1. Their areas are as follows: 140.9 mm^2, 803.8 mm^2, 2491 mm^2, and 3391 mm^2.

The input pressure is arbitrary since the model is linear. A constant value of 100 Pa was used for both models and applied normal to the surface for both TB and TM models.

In both models, the distal edges of the suspensory soft tissues (the posterior incudal ligament at its connection to the periotic bone and the stapedius tendon at its connection to the muscle body) were fixed. The connections to the periotic bone (the outer edge of the annular ligament and the two bony attachments of the tympanic bone on either side of the sigmoid process) were also fixed. These regions are illustrated in Fig. 1.

Rayleigh damping, a type of damping that is mass- and stiffness-proportional, was applied to all geometry within the model. The damping parameters used were as follows: damping coefficient α, $1 \times 10^3\ s^{-1}$; and damping coefficient β, 1×10^{-5} s. Coefficient β was chosen to be on the order of that used in other auditory FE models (e.g., Koike *et al.*, 2002; Gan *et al.*, 2004). Coefficient α was chosen to minimize resonances in the middle ear response. Cochlear damping was applied to the stapes footplate using the same cochlear damping constant, 0.217 N s/m, from Tubelli *et al.* (2012).

Output of the model was taken as the output velocity at the central node of the stapes footplate divided by input pressure, giving a frequency-dependent transfer function with the units of nm/Pa s.

III. EXPERIMENTAL COMPARISON

In an effort to validate the model, we experimentally measured the middle ear frequency response of a *M. novaeangliae* ear. The specimen employed (Mnov22, Table I) was a left ear obtained from a code 3 (low to moderate decomposition) stranded adult male humpback whale. The periotic bone of the ear was fixed to an air-cushioned vibration isolation table and a mechanical transducer was used to stimulate the ear. A vibrometer was used to measure the velocity of several points of the ear complex. Immobilizing the periotic bone reduces motion in the cochlear labyrinth components, the annular ligament, and the bony symphysis between the periotic and tympanic bones, approximating a fixed boundary condition paralleling the model. The experiment was performed in air, not underwater due to equipment limitations. The methods used are similar to experimental measurements on odontocete ears in Zosuls *et al.* (2015), except a low-frequency transducer was implemented to increase the signal-to-noise ratio at lower frequencies. The bandwidth ranged from 2 Hz to 5 kHz.

Figure 2(a) shows a block diagram of the experimental setup. MATLAB (MathWorks, Inc., Natick, MA) scripts were used to generate stimuli and run the experiments. Forty logarithmically spaced sinusoidal stimuli were synthesized with a National Instruments PCI-6052 16-bit data acquisition card (National Instruments, Austin, TX). A 25 kHz low-pass filter was used to reconstruct the stimuli which were sent to a Hafler DH200 power amplifier (Hafler, Port Coquitlam, Canada). The transducer driven by the amplifier consisted of a modified loudspeaker (Dayton Audio, Springboro, OH) with a threaded aluminum coupler bonded to the voice coil.

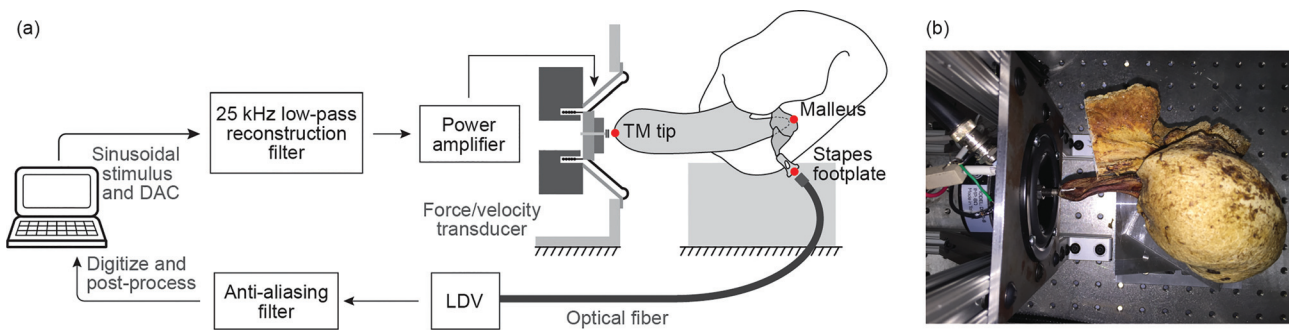

FIG. 2. (a) Block diagram of the experimental setup. Also shown are measurement locations (red dots). (b) Photo of the sample in place on the vibration isolation table coupled to loudspeaker setup.

The tympanic membrane was fixed to the coupler with cyanoacrylate adhesive (Great Planes Model Manufacturing, Champaign, IL) as shown in Fig. 2(b). Once the bond was cured, the tympanic membrane was placed in tension by retracting the loudspeaker from the ear while maintaining the voice coil in the speaker magnet to maintain speaker linearity. Cyanoacrylate adhesive and clamps were then added to fix the sample to a custom machined ear holder that was bolted to the vibration isolation table. During the experiment, the ear was irrigated with 0.9% phosphate buffered saline to maintain its condition.

A laser Doppler velocimeter (LDV) (Polytec OFV-511; Polytec Inc., Hudson, MA) was used to measure velocity at multiple locations: the manubrium of the malleus, the center of the stapes footplate, and the loudspeaker voice coil. The loudspeaker voice coil measurement was taken as the input to the system given the strong bond between to the voice coil assembly and the sample; i.e., the tip of the tympanic membrane was assumed to have the same velocity as the voice coil at the stimulus frequencies used. The output of the LDV was conditioned with a Tucker Davis FT6 low-pass filter with a corner frequency of 125 kHz followed by a Tektronix AM502 (Tektronix, Inc., Beaverton, OR) anti-aliasing filter and amplifier before it was digitized at a sampling rate of 80.6 kHz with the National Instruments PCI-6052. The digitized data was fast Fourier transformed and the stimulus frequency point was extracted to determine the magnitude and phase.

To ensure the measurements at the stapes and malleus were not an artifact of the whole ear vibrating, reference velocity measurements were taken in two places: on the periotic bone by the oval window within 3 mm of the stapes footplate and on the medial wall of the tympanic bone.

Velocity measurements were made also with the cyanoacrylate bond from the transducer to tympanic membrane severed in order to measure air borne acoustic stimulation of the ear rather than coupled mechanical stimulation. Velocities measured with the tympanic membrane decoupled were undetectable from the noise floor.

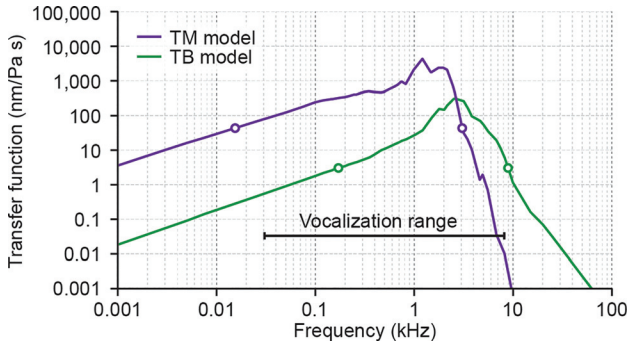

FIG. 3. Transfer function curves for the TM and TB models. The low and high cutoffs for ranges of best hearing for each model, as determined by the range of sensitivities within −40 dB of the peak values, are indicated with circles for each METF. The dominant frequency range of vocalizations for humpback whale songs is also given for comparison (see Wartzok and Ketten, 1999).

IV. RESULTS

A. Main models

Figure 3 shows the humpback whale METF for both the TB and TM models. The peak frequency for the TM model occurs between 1 and 2 kHz with a high-frequency slope that drops off sharply at 100 dB/decade after the peak. The peak frequency of the TB METF occurs around 3 kHz, higher in frequency than for the TM model, but one order of magnitude lower, with a drop-off of 80 dB/decade. The best frequency ranges from both models coincide with known peak vocalization frequencies for humpback whale songs.

B. Model sensitivity analysis

Sensitivity analysis was performed on the Young's moduli of soft tissue (posterior incudal ligament, stapedial tendon, and the two joints), annular ligament, and tympanic membrane to determine their effects on the METF (Fig. 4).

For the TB model, an increase in soft tissue Young's modulus produces a larger bandwidth, between 200 Hz and

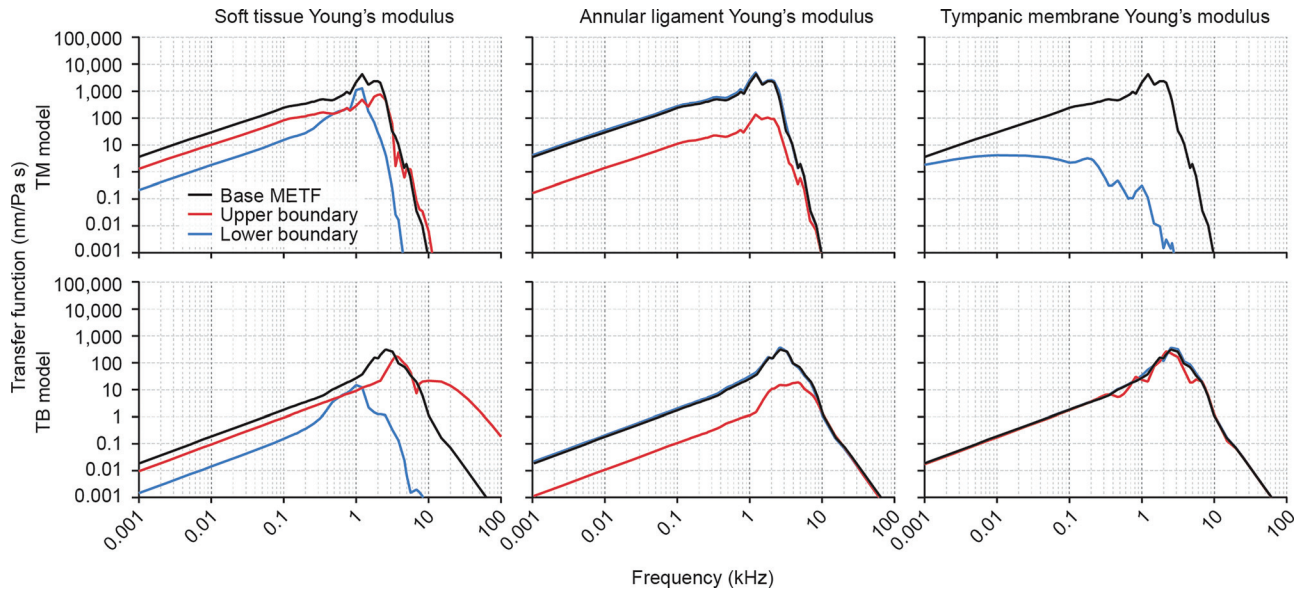

FIG. 4. Sensitivity analysis of the TM and TB models to soft tissue, annular ligament, and tympanic membrane Young's moduli.

50 kHz, whereas a decrease in soft tissue Young's modulus reduces the bandwidth to between 100 Hz and 4 kHz. The peaks are also shifted up in frequency to 3.5 kHz and down in frequency to 1 kHz when increasing and decreasing soft tissue Young's modulus, respectively. For the TM model, a higher soft tissue Young's modulus yields a peak shift to slightly above 2 kHz, while a lower soft tissue Young's modulus does not yield a peak shift. In both cases, increasing and decreasing soft tissue Young's modulus results in the METF generally decreasing in magnitude.

In both models, decreasing the annular ligament Young's modulus has an insignificant effect on the METF. Increasing the annular ligament Young's modulus decreases the METF by an order of magnitude for both models up to 8 kHz, above which the METFs generally remain unchanged.

Decreasing Young's modulus of the tympanic membrane has a significant effect on the TM model METF by attenuating mid and high frequencies, removing the peak entirely. Increasing the tympanic membrane Young's modulus to the upper limit of 9×10^8 Pa causes such a dramatic decrease in the TM model METF magnitude that the entire curve is below the plotted range of magnitude values. Decreasing Young's modulus of the tympanic membrane for the TB model has no effect on the METF; increasing Young's modulus introduces some resonances between 200 Hz and 7 kHz, but the METF shape remains otherwise unchanged.

In general, a larger input pressure area on the tympanic membrane in the TM model results in a higher magnitude and a shift in the peak to a higher frequency, whereas a smaller input area has the opposite effect on the METF (Fig. 5). Within the range of tested values, from the tip of the tympanic membrane to the length of the tympanic membrane external to the middle ear cavity, the peak shifted between 800 Hz to 2 kHz.

C. Experimental results

Figure 6 shows the velocity magnitude transfer functions for the model and the experiment. The transfer function outputs were the manubrium of the malleus and the stapes footplate. The velocities measured are the result of a pressure input on the tip of the tympanic membrane. In the experiments, the tip of the tympanic membrane was coupled to a force. The model curves in Fig. 6 were generated with the material property values in Table II and an input surface

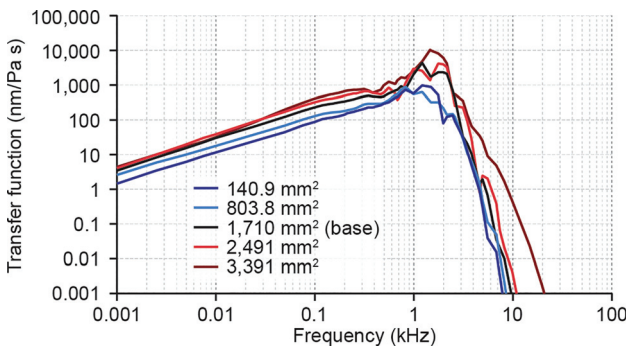

FIG. 5. Sensitivity analysis of the TM model to input area.

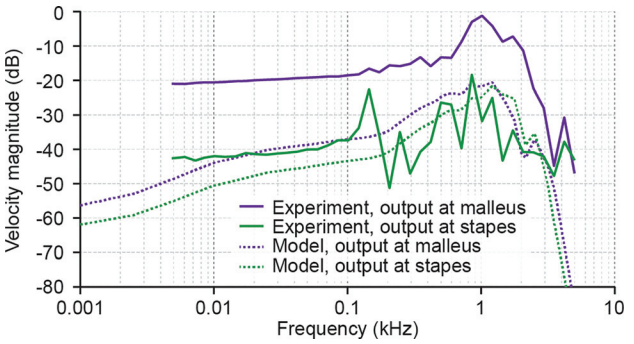

FIG. 6. A comparison of the middle ear output velocity relative to input velocity for the experiment and model. Velocity was measured at the tympanic membrane tip, the manubrium of the malleus, and the stapes footplate when the tympanic membrane was driven with a pressure source. The velocity magnitude in dB is relative to the tympanic membrane. To reproduce the experiment more accurately, the surface area of the model pressure source was matched to the area of the stimulator connection in the experiment.

area at the tip of the tympanic membrane that was similar to that of the aluminum coupler in the experiment. The experiment yields a nearly perfect efficiency of the velocity transfer from the tympanic membrane tip to its insertion on the malleus at 1 kHz. The model displays a peak efficiency close to 1 kHz corresponding to the TM model METF peak. The magnitude differences between the two outputs are more pronounced in the experiments than for the models.

V. DISCUSSION

We can test the validity of the humpback whale METF by considering the resultant velocity at the stapes footplate at estimated hearing thresholds compared to those measured in terrestrial mammals. The hearing threshold was estimated to be 70 dB re 1 μPa based on odontocete audiograms (Johnson, 1968; Szymanski *et al.*, 1999). Multiplying the METF by the pressure at the 70 dB threshold (0.003162 Pa) results in a stapes velocity of 24 nm/s at the most sensitive region in the METF. This velocity is similar to other species as shown in Tubelli *et al.* (2012).

Characteristic "song" vocalizations of humpback whales range from 40 Hz up to 4 kHz for the dominant frequencies. The best hearing range, based on −40 dB from the peak transfer function magnitude, predicted by the TM model is between 15 Hz and approximately 3 kHz. The TB model predicts a best hearing range of 200 Hz to approximately 9 kHz. Thus, a composite of the two model results essentially cover the entire range of vocalization frequencies described in the current literature and are consistent with the peak spectra of the vocalization data (Wartzok and Ketten, 1999).

The shapes of the METF for humpback whale from this study and for minke whales from Tubelli *et al.* (2012) are similar. The minke METF has more resonances that can be attributed to a lower Rayleigh damping coefficient α used in that model. Humpback best hearing range is predicted to have an upper-frequency cutoff of 3 kHz, lower than that of the minke whale at 7.5 kHz, with stimulation at the tympanic membrane. Similarly, stimulation at the tympanic bone yields an upper-frequency cutoff of 9 kHz compared to 25 kHz for the minke whale ear. This result is supported by

the observation in terrestrial mammals that more massive ossicles, as found in the humpback whale, correlate with improved hearing at lower frequencies. The malleus in the humpback ear is about twice the mass of the minke malleus, although both have a similar geometry. These differences are also supported by vocalization frequencies: from 40 Hz to 4 kHz for humpback (Wartzok and Ketten, 1999) and 50 Hz to 9.4 kHz for minke (Gedamke *et al.*, 2001).

For material properties that have no experimental measurements, estimated values were used for modeling. The importance of those values was elucidated with sensitivity analysis in which parametric values could be anywhere within the physiological range. The wide range of Young's moduli of soft tissues in general is shown to have an effect on both the bandwidth and peak frequencies within the model, affirming that direct measurements of Young's moduli for all auditory soft tissues, especially that of the tympanic membrane, are necessary to achieve a more accurate model.

Although the experimental velocity transfer functions do not align with those of the model, there are some similarities. The stapes experiment and model transfer functions align better in magnitude than the malleus experiment and model transfer functions. They are similar in that both peak in the 1 kHz region and the high-frequency cutoffs and slopes match. The low-frequency slopes, however, vary. The model slope is 7.3 dB/decade, whereas the experimental data slope is 2.1 dB/decade. For both experiment and model, on average, the stapes amplitude was less than that of the malleus. The slopes for the malleus and stapes within the model and experiment are consistent in the low-frequency region. The stapes magnitude in the experiment was considerably diminished relative to the malleus. While we cannot with certainty explain the differences in the curves between model and experimental data, we can potentially explain them as parameter changes in the experimental ear because postmortem tissue quality was necessarily compromised compared to the expected values employed in the model. It is possible that the interossicular joints were subjected to degradation, thus reducing the energy transfer efficiency. If this was the case, the contribution of the stapes annular ligament and ossicular mass to the mechanical impedance of the ossicular chain would be attenuated from the point of view of a pressure source at the tympanic membrane. Additionally, the tympanic membrane appeared quite stiff in comparison to the other soft tissues, suggesting the value of Young's modulus used in the model may be too low. If these concerns were modeled in the form of decreasing the incudostapedial joint by two orders of magnitude and increasing Young's modulus of the tympanic membrane by one order of magnitude, the resultant model velocity transfer function curves are more in line with those measured experimentally (Fig. 7). One other point is that anisotropy of the bone could play a role in the complex motion of the ossicles that a single value of Young's modulus cannot fully capture, leading to changes in the transfer function.

The hearing apparatus in mammals is a bandpass system. The middle ear component of the audiogram, represented by the transfer function, is a major contributor to the

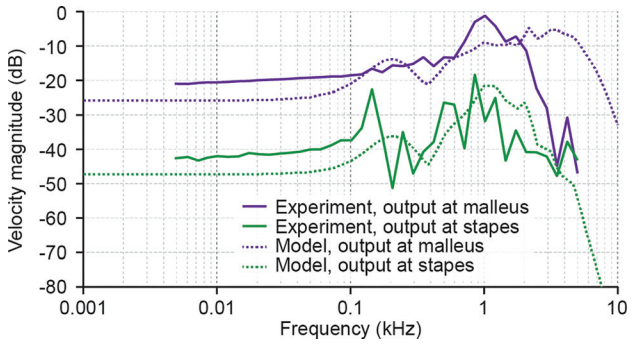

FIG. 7. A comparison of the middle ear output velocity relative to input velocity for the experiment and model where Young's modulus for the model incudostapedial joint was decreased two orders of magnitude to simulate joint deterioration and Young's modulus for the tympanic membrane was increased one order of magnitude to simulate a stiffer material. Velocity was measured at the tympanic membrane tip, the manubrium of the malleus, and the stapes footplate when the tympanic membrane was driven with a pressure source. Velocity magnitude is relative to the tympanic membrane.

frequency response shape of the hearing threshold (Ruggero and Temchin, 2002). This likely reflects the audiogram peak sensitivities; however, this is only one component, in which the external and inner ears form additional components with each of the contributing important elements to the audiogram. The steeper low-frequency cutoff of an audiogram compared to a METF can possibly be attributed to the effect of the helicotrema acting as a low-impedance pressure loss in the cochlea at low frequencies. Low impedance means the helicotrema, which is a conduit, variable in shape and three-dimensional, allows fluid flow from scala vestibuli to scala tympani at low frequencies. The effect increases at low frequencies because at high frequencies the length and cross section of the scalae cause the fluid in the cochlea to act as a mass (Dallos, 1970). This mass load impedes the flow of fluid at the apex thus the pressure release is through the cochlear partition.

While we believe that these models are the best that can be achieved at present and include all key features and pathways of the whale peripheral auditory system, there are several caveats. The hearing system is much more complex than our model allows. Many other tissues abutting the geometry we modeled here would certainly have an effect on the results, including the material properties of the periotic bone, its fluid and membranous labyrinths, and the nature of its attachments to the tympanic bone and the middle ear soft tissues as well as the fats adjacent to the tympano-periotic complex and the wax cap that abuts the tympanic membrane. The tissues we received were not suitable for studying the lipid elements in particular, reliably or in detail. The wax cap is unique in mysticetes and is a rarely found element of this system that may have a role in function and reception and certainly deserves further exploration.

Our comparison of the model and experimental data underscores the importance of appreciating and assessing the limitations imposed by the quality and handling of postmortem tissues and the importance of multiple repeat measures on more than one specimen for any species. Therefore, just as adding additional measures of the material properties of each element increases validity, being able to add both

realistic elements through more features and properties and in more mysticete species is a critical step for a comprehensive answer to mysticete hearing. Any guesses about the material properties and structures of elements, like the wax cap and peribullar fats, raise associated concerns for omissions or errors in model results. In parallel, drawing conclusions solely from a single measure of an imperfect ear can lead to misestimates. Performing transfer function measurements on more ears in better condition will improve the confidence and comparison of model and actual tissue measures. Even more important, as the variations between minke and humpback data show clearly, through the application of parallel techniques and analyses, simple extrapolations from one species to another are inappropriate and lumping all mysticetes into one hearing category is unlikely to be valid.

Another caveat is the uncertainty of input into the middle ear. There are two potential inputs based on the theories put forth for cetacean hearing (conventional tympanic membrane and ossicular motion vs bone conduction) (see Ketten, 2000 for discussion). Inertial movement of the tympanic relative to the periotic resulting in ossicular motion has been proposed by previous publications (Fleischer, 1978; McCormick *et al.*, 1970; Hemilä *et al.*, 1995; Cranford and Krysl, 2015). This mode relies on differential displacement of the skull and the tympanic bone, which has not been demonstrated for acoustic stimuli and is contrary to best stimulation sites with jawphone experiments on odontocetes (Brill, 1988; Popov and Supin, 1990; Møhl *et al.*, 1999; Brill *et al.*, 2001; Mooney *et al.*, 2013). No data to date have specifically tested either input for mysticetes.

Of the two inputs tested, the highly-specialized tympanic membrane appears to be the more likely acoustic input rather than tympanic bone motion, as the fibrous tissue of the tympanic membrane is connected to and consistent with direct motion of the ossicles.

The tympanic bone may seem to respond well here, but we are using a mechanical pressure. Based on the theory for odontocetes and the known anatomy, the pressure is not mechanical but rather acoustic, propagating through specialized fats and into the cavity of the tympano-periotic complex. Properties of these fats, including their acoustic properties, have been explored in some cetaceans (Koopman *et al.*, 2006; Prasad, 2003; Yamato *et al.*, 2012) but still require further investigation to properly understand their material and acoustic properties. An acoustic signal is likely to be reflected from bone, if that were the primary input, resulting in a substantial attenuation of any signal via bone conduction alone. Further, we have not found an example in which jaw fats are not connected to the tympanic membrane. Nevertheless, we considered and tested the bone conduction theory through stimulation of the tympanic bone alone in the TB model as described above and found it inferior to tympanic membrane stimulation with respect to magnitude of response. Further, sound speeds in the jaw fats are slower, which is highly suggestive of a preferential water-adapted low impedance channel to the tympanic membrane just as the air-filled external auditory canal is the lowest impedance channel in air-adapted mammalian ears.

No mammal is known to have bone conduction as the primary pathway of sound to the ear. While some mammals can sense sound via bone conduction, it is considered an auxiliary path that in some lower animals is effective but is superseded by ossicular paths in mammals (Manley and Sienknecht, 2013). As Hood (1962) stated in his summary of fundamental bone conduction research, von Békésy showed "the evolutionary development of the ossicular chain would appear to be directed towards reducing bone conducted sounds to a minimum." Further, thresholds by bone conduction are diminished by as much as 75 dB (von Békésy, 1948, 1949). Recent results show that while basilar membrane vibrations can be initiated via bone conduction, cochlear fluid pressures differ substantially based on the mode of the excitation, consistent with von Békésy's observations (Kim *et al.*, 2011). There are speculations that bone conduction may provide enhanced input for lower frequencies (Stenfelt, 2013) but there are additional concerns that such a path would, particularly in water, hamper localization and discrimination. We cannot reasonably conclude based on currently available data that bone conduction would be a preferential pathway in whales either, given normal acoustic source levels.

VI. CONCLUSIONS

Knowledge of the hearing of mysticetes is critical to understanding how these aquatic animals, many of which are seriously endangered, may be affected by anthropogenic noise. The METF obtained by FE modeling of the humpback whale ear and direct experimentation on a cadaveric ear that we present are one part of a series of anatomical and direct experiments we are pursuing to provide a composite estimate of the hearing characteristics for this and other marine mammal species.

In this study, an anatomically accurate model of the humpback whale middle ear was created, incorporating both bone and soft tissues. The resulting FE transfer function displays a better frequency range for the humpback whale between approximately 15 Hz and 3 kHz when stimulated at the tympanic membrane, and between approximately 200 Hz and 9 kHz if stimulated at the thinner region of the tympanic bone adjacent to the tympanic membrane.

ACKNOWLEDGMENTS

The authors acknowledge the support of the Joint Industry Program for Sound in the Sea, the Seaver Institute, the Hanse-Wissenschaftskollegg, the Helmholtz Association, and Living Marine Resources Program. We thank Scott Cramer and Julie Arruda for extensive technical assistance, Cody Yardley for assisting with the experimental setup, and Dr. H. Steven Colburn for his support. We also wish to thank Kimberly Durham, Katie Moore, Misty Niemeyer, Aleta Hohn, and Jennifer Skidmore for their assistance and guidance in obtaining specimens and permitting processes as well as the responders and volunteers of the Marine Mammal Health and Stranding Response Program, the Riverhead Foundation for Marine Research, the International Fund for Animal Welfare (IFAW), and the

National Oceanic and Atmospheric Administration, without which this research would not have been possible. We also wish to acknowledge the guidance and insights of our co-author, Dr. David Mountain, who was so very important to all of our work and who is sorely missed by all of us as well as his colleagues at Boston University and elsewhere.

Au, W. W., Pack, A. A., Lammers, M. O., Herman, L. M., Deakos, M. H., and Andrews, K. (**2006**). "Acoustic properties of humpback whale songs," J. Acoust. Soc. Am. **120**(2), 1103–1110.

Brill, R. L. (**1988**). "The jaw-hearing dolphin: Preliminary behavioral and acoustical evidence," in *Animal Sonar*, edited by P. E. Nachtigall and P. W. B. Moore (Springer, Boston, MA), pp. 281–287.

Brill, R. L., Moore, P. W., and Dankiewicz, L. A. (**2001**). "Assessment of dolphin (*Tursiops truncatus*) auditory sensitivity and hearing loss using jawphones," J. Acoust. Soc. Am. **109**(4), 1717–1722.

Chandrashekar, N., Mansouri, H., Slauterbeck, J., and Hashemi, J. (**2006**). "Sex-based differences in the tensile properties of the human anterior cruciate ligament," J. Biomech. **39**(16), 2943–2950.

Clark, C. W. (**1990**). "Acoustic behavior of mysticete whales," in *Sensory Abilities of Cetaceans*, edited by J. A. Thomas and R. A. Kastelein (Plenum, New York), pp. 571–583.

Cranford, T. W., and Krysl, P. (**2015**). "Fin whale sound reception mechanisms: Skull vibration enables low-frequency hearing," PloS One **10**(1), e0116222.

Dallos, P. (**1970**). "Low-frequency auditory characteristics: Species dependence," J. Acoust. Soc. Am. **48**(2), 489–499.

Dallos, P. (**1973**). *The Auditory Periphery: Biophysics and Physiology* (Academic, New York).

De Greef, D., Pires, F., and Dirckx, J. J. (**2017**). "Effects of model definitions and parameter values in finite element modeling of human middle ear mechanics," Hear. Res. **344**, 195–206.

Dooling, R. J., Peters, S. S., and Searcy, M. H. (**1979**). "Auditory sensitivity and vocalizations of the field sparrow (*Spizella pusilla*)," Bull. Psychonom. Soc. **14**(2), 106–108.

Ekdale, E. G., Berta, A., and Deméré, T. A. (**2011**). "The comparative osteology of the petrotympanic complex (ear region) of extant baleen whales (Cetacea: Mysticeti)," PloS One **6**(6), e21311.

Fleischer, G. (**1978**). "Evolutionary principles of the mammalian middle ear," Adv. Anat. Embryol. Cell Biol. **55**(5), 3–70.

Fraser, F. C., and Purves, P. E. (**1954**). "Hearing in cetaceans," Bull. Br. Museum **2**(5), 103–116.

Fraser, F. C., and Purves, P. E. (**1960**). "Anatomy and function of the cetacean ear," Proc. R. Soc. Lond. Ser. B: Biol. Sci. **152**(946), 62–77.

Gan, R. Z., Feng, B., and Sun, Q. (**2004**). "Three-dimensional finite element modeling of human ear for sound transmission," Ann. Biomed. Eng. **32**(6), 847–859.

Gedamke, J., Costa, D. P., and Dunstan, A. (**2001**). "Localization and visual verification of a complex minke whale vocalization," J. Acoust. Soc. Am. **109**(6), 3038–3047.

Hashemi, J., Chandrashekar, N., and Slauterbeck, J. (**2005**). "The mechanical properties of the human patellar tendon are correlated to its mass density and are independent of sex," Clin. Biomech. **20**(6), 645–652.

Hemilä, S., Nummela, S., and Reuter, T. (**1995**). "What middle ear parameters tell about impedance matching and high frequency hearing," Hear. Res. **85**(1–2), 31–44.

Homma, K., Du, Y., Shimizu, Y., and Puria, S. (**2009**). "Ossicular resonance modes of the human middle ear for bone and air conduction," J. Acoust. Soc. Am. **125**(2), 968–979.

Homma, K., Shimizu, Y., Kim, N., Du, Y., and Puria, S. (**2010**). "Effects of ear-canal pressurization on middle-ear bone- and air-conduction responses," Hear. Res. **263**(1), 204–215.

Hood, J. D. (**1962**). "Bone conduction: A review of the present position with especial reference to the contributions of Dr. Georg von Békésy," J. Acoust. Soc. Am. **34**, 1325–1332.

Johnson, C. S. (**1968**). "Sound detection thresholds in marine mammals," in *Marine Bioacoustics*, edited by W. N. Tavolga (Pergamon, New York), Vol. 2, pp. 247–260.

Ker, R. F. (**1981**). "Dynamic tensile properties of the plantaris tendon of sheep (*Ovis aries*)," J. Exp. Biol. **93**(1), 283–302.

Ketten, D. R. (**1992**). "The marine mammal ear: Specializations for aquatic audition and echolocation," in *The Evolutionary Biology of Hearing*, edited by D. B. Webster, A. N. Popper, and R. R. Fay (Springer, New York), pp. 717–750.

Ketten, D. R. (**1994**). "Functional analyses of whale ears: Adaptations for underwater hearing," Proc. OCEANS'94 **1**, 264–270.

Ketten, D. R. (**2000**). "Cetacean ears," in *Hearing by Whales and Dolphins*, edited by W. L. Au, A. N. Popper, and R. R. Fay (Springer, New York), pp. 43–108.

Ketten, D. R. (**2002**). "Marine mammal auditory systems: A summary of audiometric and anatomical data and implications for underwater acoustic impacts," Polarforschung **72**(2–3), 79–92.

Kim, N., Homma, K., and Puria, S. (**2011**). "Inertial bone conduction: Symmetric and anti-symmetric components," J. Assoc. Res. Otolaryngol. **12**(3), 261–279.

Koike, T., Wada, H., and Kobayashi, T. (**2002**). "Modeling of the human middle ear using the finite-element method," J. Acoust. Soc. Am. **111**(3), 1306–1317.

Koopman, H. N., Budge, S. M., Ketten, D. R., and Iverson, S. J. (**2006**). "Topographical distribution of lipids inside the mandibular fat bodies of odontocetes: Remarkable complexity and consistency," IEEE J. Ocean. Eng. **31**(1), 95–106.

Kuo, P. L., Li, P. C., and Li, M. L. (**2001**). "Elastic properties of tendon measured by two different approaches," Ultrasound Med. Biol. **27**(9), 1275–1284.

Ladich, F., and Yan, H. Y. (**1998**). "Correlation between auditory sensitivity and vocalization in anabantoid fishes," J. Compar. Physiol. A **182**, 737–746.

Lillie, D. G. (**1910**). "Observations on the anatomy and general biology of some members of the larger cetacea," Proc. Zool. Soc. Lond. **80**, 769–792.

Manley, G. A., and Sienknecht, U. (**2013**). "The evolution and development of middle ears in land Vertebrates," in *The Middle Ear: Science, Otosurgery, and Technology*, edited by S. Puria, R. R. Fay, and A. N. Popper (Springer, New York), pp. 7–30.

Manoussaki, D., Chadwick, R. S., Ketten, D. R., Arruda, J., Dimitriadis, E. K., and O'Malley, J. T. (**2008**). "The influence of cochlear shape on low-frequency hearing," PNAS **105**(16), 6162–6166.

McCormick, J. G., Wever, E. G., Palin, J., and Ridgway, S. H. (**1970**). "Sound conduction in the dolphin ear," J. Acoust. Soc. Am. **48**, 1418–1428.

McCormick, J. G., Wever, E. G., Ridgway, S. H., and Palin, J. (**1980**). "Sound reception in the porpoise as it relates to echolocation," in *Animal Sonar Systems*, edited by R.-G. Busnel and J. F. Fish (Plenum Press, New York), pp. 449–467.

McGough, R. L., Debski, R. E., Taskiran, E., Fu, F. H., and Woo, S. L. (**1996**). "Mechanical properties of the long head of the biceps tendon," Knee Surg. Sports Traumatol. Arthrosc. **3**(4), 226–229.

Mead, J. G., and Fordyce, R. E. (**2009**). "The therian skull: A lexicon with emphasis on the odontocetes," Smithson. Contrib. Zool. **627**, 1–261.

Meenderink, S. W. F., Kits, M., and Narins, P. M. (**2010**). "Frequency matching of vocalizations to inner-ear sensitivity along an altitudinal gradient in the coqui frog," Biol. Lett. **6**(2), 278–281.

Møhl, B., Au, W. W. L., Pawloski, J., and Nachtigall, P. E. (**1999**). "Dolphin hearing: Relative sensitivity as a function of point of application of a contact sound source in the jaw and head region," J. Acoust. Soc. Am. **105**(6), 3421–3424.

Mooney, T. A., Li, S., Ketten, D., Wang, K., and Wang, D. (**2013**). "Hearing pathways in the Yangtze finless porpoise, Neophocaena asiaeorientalis asiaeorientalis," J. Exp. Biol. **217**, 444–452.

Norris, K. S. (**1968**). "The evolution of acoustic mechanisms in odontocete cetaceans," in *Evolution and Environment*, edited by E. T. Drake (Yale University Press, New Haven), pp. 297–324.

Nummela, S., Wägar, T., Hemilä, S., and Reuter, T. (**1999**). "Scaling of the cetacean middle ear," Hear. Res. **133**(1), 71–81.

Olson, E. S. (**1998**). "Observing middle and inner ear mechanics with novel intracochlear pressure sensors," J. Acoust. Soc. Am. **103**(6), 3445–3463.

Overstreet, E. H., III, and Ruggero, M. A. (**2002**). "Development of wide-band middle ear transmission in the Mongolian gerbil," J. Acoust. Soc Am. **111**(1), 261–270.

Payne, K., Tyack, P., and Payne, R. (**1983**). "Progressive changes in the songs of humpback whales (Megaptera novaeangliae): A detailed analysis of two seasons in Hawaii," in C*ommunication and Behavior of Whales*, edited by R. S. Payne (AAAS Selected Symposium, Boulder, CO), pp. 9–57.

Pilleri, G. C., Kraus, C., and Gihr, M. (**1987**). "The organ of hearing in cetaceans 1: Recent species," Invest. Cetacea **20**, 43–177.

Popov, V., and Supin, A. (**1990**). "Localization of the acoustic window at the dolphin's head," in *Sensory Abilities of Cetaceans*, edited by J. A. Thomas and R. A. Kastelein (Springer, Boston, MA), pp. 417–426.
Prasad, K. (**2003**). "Sound speed investigation of dolphin tissue," Master's thesis, University of Massachusetts, Dartmouth, MA.
Provenzano, P. P., Lakes, R. S., Corr, D. T., and Vanderby, R. (**2002**). "Application of nonlinear viscoelastic models to describe ligament behavior," Biomech. Model. Mechanobiol. **1**(1), 45–57.
Purves, P. E. (**1955**). "The wax plug in the external auditory meatus of the Mysticeti," Discov. Rep. **27**, 293–302.
Qi, L., Liu, H., Lutfy, J., Funnell, W. R. J., and Daniel, S. J. (**2006**). "A nonlinear finite-element model of the newborn ear canal," J. Acoust. Soc. Am. **120**(6), 3789–3798.
Ravicz, M. E., Cooper, N. P., and Rosowski, J. J. (**2008**). "Gerbil middle-ear sound transmission from 100 Hz to 60 kHz," J. Acoust. Soc. Am. **124**(1), 363–380.
Rosowski, J. J. (**1991**). "The effects of external- and middle-ear filtering on auditory threshold and noise-induced hearing loss," J. Acoust. Soc. Am. **90**(1), 124–135.
Ruggero, M. A., and Temchin, A. N. (**2002**). "The roles of the external, middle, and inner ears in determining the bandwidth of hearing," Proc. Natl. Acad. Sci. **99**(20), 13206–13210.
Silber, G. K. (**1986**). "The relationship of social vocalizations to surface behavior and aggression in the Hawaiian humpback whale (Megaptera novaeangliae)," Can. J. Zool. **64**(10), 2075–2080.
Stäubli, H. U., Schatzmann, L., Brunner, P., Rincón, L., and Nolte, L. P. (**1999**). "Mechanical tensile properties of the quadriceps tendon and patellar ligament in young adults," Am. J. Sports Med. **27**(1), 27–34.
Stenfelt, S. (**2013**). "Bone conduction and the middle ear," in *The Middle Ear: Science, Otosurgery, and Technology*, edited by S. Puria, R. R. Fay, and A. N. Popper (Springer, New York), pp. 135–169.
Szymanski, M. D., Bain, D. E., Kiehl, K., Pennington, S., Wong, S., and Henry, K. R. (**1999**). "Killer whale (Orcinus orca) hearing: Auditory brainstem response and behavioral audiograms," J. Acoust. Soc. Am. **106**(2), 1134–1141.
Thompson, P. O., Cummings, W. C., and Ha, S. J. (**1986**). "Sounds, source levels, and associated behavior of humpback whales, Southeast Alaska," J. Acoust. Soc. Am. **80**(3), 735–740.
Tubelli, A. A., Zosuls, A., Ketten, D. R., and Mountain, D. C. (**2014**). "Elastic modulus of cetacean auditory ossicles," Anatom. Rec. **297**(5), 892–900.
Tubelli, A. A., Zosuls, A., Ketten, D. R., Yamato, M., and Mountain, D. C. (**2012**). "A prediction of the minke whale (Balaenoptera acutorostrata) middle-ear transfer function," J. Acoust. Soc. Am. **132**(5), 3263–3272.
Tuck-Lee, J. P., Pinsky, P. M., Steele, C. R., and Puria, S. (**2008**). "Finite element modeling of acousto-mechanical coupling in the cat middle ear," J. Acoust. Soc. Am. **124**(1), 348–362.
von Békésy, G. (**1948**). "Vibrations of the head in a sound field and its role in hearing by bone conduction," J. Acoust. Soc. Am. **20**, 749–760.
von Békésy, G. (**1949**). "The structure of the middle ear and the hearing of one's own voice by bone conduction," J. Acoust. Soc. Am. **21**(3), 217–232.
Wang, X., and Gan, R. Z. (**2016**). "3D finite element model of the chinchilla ear for characterizing middle ear functions," Biomech. Model. Mechanobiol. **15**(5), 1263–1277.
Wartzok, D., and Ketten, D. R. (**1999**). "Marine mammal sensory systems," in *Biology of Marine Mammals*, edited by J. Reynolds and S. Rommel (Smithsonian Institution Press, Washington, D.C.), pp. 117–175.
Yamada, M. (**1953**). "Contribution to the anatomy of the organ of hearing of whales," Sci. Rep. Whales Res. Inst. **8**, 1–79.
Yamato, M., Ketten, D. R., Arruda, J., Cramer, S., and Moore, K. (**2012**). "The auditory anatomy of the minke whale (Balaenoptera acutorostrata): A potential fatty sound reception pathway in a baleen whale," Anatom. Rec. **295**(6), 991–998.
Zosuls, A., Mountain, D. C., and Ketten, D. R. (**2015**). "How is sound conducted to the cochlea in toothed whales?," AIP Conf. Proc. **1703**(1), 060006.